

## Symmetric Waveguide Orthomode Junctions

E.J. Wollack<sup>1</sup> and W. Grammer<sup>2</sup>

National Radio Astronomy Observatory<sup>2</sup>  
949 North Cherry Avenue, Tucson, AZ 85721

Laboratory for Astronomy and Astrophysics<sup>1</sup>  
NASA/Goddard Space Flight Center  
Greenbelt, MD 20771  
email: edward.wollack.1@gsfc.nasa.gov

**ABSTRACT** – Imaging applications at millimeter and submillimeter wavelengths demand precise characterization of the amplitude, spectrum, and polarization of electromagnetic radiation. The use of a waveguide orthomode transducer (OMT) can help achieve these goals by increasing spectral coverage and sensitivity while reducing exit aperture size, optical spill, instrumental polarization offsets, and lending itself to integration in focal plane arrays. For these reasons, symmetric OMTs are favored over a traditional quasi-optical wire grid for focal plane imaging arrays from a systems perspective. The design, fabrication, and test of OMTs realized with conventional split-block techniques for millimeter-waveguide bands are described. The design provides a return loss of ~20 dB over a full waveguide band. The observed cross-polarization and isolation are better than ~40 dB for tolerances readily achievable in practice. Prototype examples realized in WR10.0 and WR3.7 waveguide bands are presented.

**Keywords:** Orthomode Transducer, Polarization Diplexer, Waveguide Techniques

### INTRODUCTION:

Receiver systems for radio astronomy require high-performance polarization-discrimination components. We report on the fabrication and performance of a wideband linear polarization diplexer for millimeter wavelengths. The designs considered here build on the concepts laid out by Brain (1978) at the Marconi Research Laboratory and first reported in a true split-block configuration by Boifot (1991). This two-fold symmetric junction achieves full waveguide band performance by limiting the excitation

of  $TE_{11}$  and  $TM_{11}$  in the square common-port. This was a key step toward the development of a wide bandwidth topology amenable to manufacture at millimeter wavelengths. These properties have led to use of this configuration in full-waveguide band receivers at centimeter and millimeter wavelengths (Cazzatello et al., 1996; Wollack, 1996). More recently, variations on these ideas have been explored with machinable apertures replacing the discrete compensation pins (Narayanan & Erickson, 2002; Nesti, 2002). In addition, see Uher, et al. (1993) for a comprehensive review of wide- and narrow-band OMT designs.

The two-fold symmetric OMT can be viewed as a variant on the turnstile junction where two of the ports have been folded parallel to the common-port [4]. The two ports that form the main-arm are separated by a thin septum, combined, and transformed to standard-height waveguide. For the other polarization, this septum forms a pair of back-to-back "mitered" bends which feed the symmetric side-arm ports. The pin number, diameter, and location are a compromise between tuning the septum reactance produced in the side-arm ports and allowing a low impedance return path for the main-arm currents.

To lowest order, throughout the structure, the propagation constant and impedance are constant. Although other implementations can be envisioned, this approach minimizes the frequency dispersion between the output ports. The main and side-arm junctions are two-fold symmetric about the horizontal and vertical guide planes, thus,  $TE_{11}$  and  $TM_{11}$  excitation can be avoided in the square common-arm of the junction to the extent that this condition is realized during fabrication and assembly.

This polarizer configuration can achieve relatively low fabrication cost while maintaining superior full waveband performance. The key strengths of this approach are as follows:

Fabrication:	2-piece split-block
Design Bandwidth:	$1.15 < f / f_c < 1.95$
Return Loss:	~ 20dB (typical) at millimeter wavelengths
Isolation:	> 40dB (typical); limited by symmetry of junction
Phase Balance:	< 20deg phase error (typical); $1.2 < f / f_c < 1.9$

We observe that the broadband phase balance is a direct consequence of the homogenous propagation constant in the structure. The functional form of the residual phase error is approximately parabolic with frequency.<sup>1</sup> For broadband polarimetry, these properties have the potential to enable a substantial improvement in continuum receiver technology over current approaches.

---

<sup>1</sup> This has been experimentally verified in the present design topology by equalizing the side- and main-arm path lengths with a waveguide shim and measuring the phase difference between the two output ports.

### Symmetric OMTs: $\lambda \approx 3\text{mm}$ and 1mm Designs

We present details for prototype 3mm and 1mm two-fold symmetric waveguide OMTs. See Table 1 for a summary of mechanical specifications. A W-band (ALMA Band-3) prototype device with standard 3/4"-round flange interfaces is depicted in Figure 1. To achieve clearance between the side- and main-arm port flanges, the side-arm power combiner was realized at the interface of a 1:1 to 2:1 transition and a 65° miter was used in the main-arm port. This miter design provides full waveguide-band performance without the discontinuity jutting above the plane of the split-block and minimized the guide lengths for the indicated constraints. This was convenient for testing the basic properties of the prototype junction. The mixer block to OMT interface will determine the final package geometry.

The side-arms were realized in 2:1 guide and are combined in a 1:1 guide which is adiabatically transformed to a standard height. Placing the impedance transformer after the side-arm power combiner relaxes the tolerances required to maintain the phase match before the signals are recombined. For additional loss considerations see Appendix A. A discrete compensation approach related by symmetry to a miter bend is employed for the side-arm power combiner as described [4,5].

The split-block housing was fabricated out of brass. The main-arm output section was defined by multiple pass EDM (Electric-Discharge-Milling). The septum was made out of 61 $\mu\text{m}$  beryllium-copper shim stock. The septum is integrated into the 2:1 Chebyshev stepped main-arm transformer. A ~100mm length of 125 $\mu\text{m}$  diameter copper-clad steel magnet wire was threaded through the holes to realize the compensation "pins". After assembling the blocks and septum, the wires are potted into the upper block and trimmed. The resulting configuration is insensitive to variation in applied force and allows disassembly of the block if desired.

The performance indicated in Figure 2 is with four pins and the nominal septum placement used to compensate the junction. Measurement frequencies are normalized to the WR10.0 cutoff,  $f_c = 59.01$  GHz, to facilitate comparison of the response. TRL (Thru-Reflect-Line) was used to calibrate the HP85106D network analyzer. The common-arm termination is a sliding conical load with a return loss ~40dB. The data presented are uncorrected for the resultant measurement errors. The observed insertion losses for

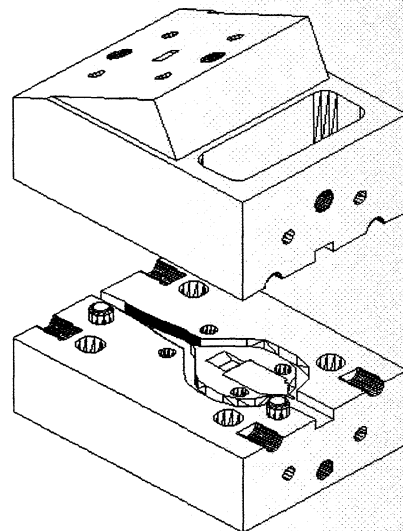


Figure 1: WR10.0 OMT Assembly.

bright and bondable pure gold plated housings are also indicated. The overall performance is in agreement with a HFSS [9] model of the structure.

The preliminary electrical characterization of a set of prototype WR03.7 full-band orthomode transducers was also performed. The design is derived from the junction previously described and is intended as a proof-of-concept for a ~1mm (ALMA Band-6) OMT. Two pairs of split-block housings were fabricated from leaded brass, to verify reproducibility of the approach. The main arm output sections on one set were formed using EDM, and on the other set by electroformed copper inserts. In a production design, the fabrication details will be modified to suit the details of the mixer block interface. The septum was produced by photolithographic etching on a 36 $\mu$ m thick beryllium-copper sheet. Copper-stainless steel magnet wire with a diameter of 61 $\mu$ m was used to compensate the junction. All components were subsequently gold plated. Further optimization of the side-arm return loss for atmospheric window is possible and would potentially result in improved overall coupling efficiency.

The measured performance indicated in Figure 3 was taken with the nominal septum placement and four wires compensating the junction. Measurement frequencies are normalized to the WR03.7 cutoff,  $f_c = 159.6$  GHz. Oleson WR03.4 millimeter-wave test set were used to measure the device's S-parameters. Data were taken both in the WR03.4 and WR03.7 waveguides with TRL (Thru-Reflect-Line) calibration. For the WR03.4 calibration, a 2:1 transition with return loss less than 25dB was used mate to the native WR03.7 OMT guide. Within the experimental error, quantitatively consistent results were obtained with both calibration approaches. The ~0.2dB ripple observed in the loss estimate results from the finite directivity of the VNA heads. The observed isolation was limited by the test set in use and will be addressed in subsequent efforts. This suite of measurements indicates that the structures have repeatable parameters during manufacture.

## **CONCLUSIONS:**

The performance of two-fold symmetric millimeter wave orthomode junctions is presented. Isolation >40 dB and return loss ~20 dB are typically observed. The ohmic contribution to the insertion loss is within a factor of ~two of the theoretical for pure gold at room temperature and improves modestly upon cooling to cryogenic temperatures. Components based upon these designs have been incorporated into state-of-the-art broadband low-noise receivers for radio astronomy. Direct integration of the OMT and sensor will be of increased importance in reaching the fundamental limits for wideband waveguide polarization applications.

**REFERENCES:**

- [1] Brain, J.M. "The Design and Evaluation of a High Performance 3 M Antenna for Satellite Communication," *The Marconi Review*, Fourth Quarter, 1978, pp. 218—236; Henderson, R.I., BAE Systems, private communication, 2002, Great Baddow, Chelmsford, UK.
- [2] Boifot, A.M., Lier, E., Schaug-Pettersen, T., "Simple and Broadband Orthomode Transducer," 1990, *Proc. IEE*, vol. 137, no. 6, pp. 396 400; Boifot, A.M., "Classification of Ortho-Mode Transducers," 1991, *European Transactions on Telecommunications and Related Technologies*, vol. 2, no. 5, pp. 503—510.
- [3] Cazzatello, G.F., Barbiero, M., Giglia, C.G.M., Klooster, C.G.M., "Wide-Band Dual-Polarized Feeds," 1996, *Workshop on Large Antennas in Radio Astronomy*, ESTEC, Noordwijk, Netherlands, pp. 159—171.
- [4] Wollack, E., "A Full Waveguide Band Orthomode Junction," 1996, NRAO, EDIR Memo Series, #303.
- [5] Wollack, E.J., Grammer, W., and Kingsley, J., "The Boifot Orthomode Junction," May 2002, NRAO, ALMA memo series #425.
- [6] Narayanan, G. and Erickson, N.R., "Design and Performance of a Novel Full-Waveguide Band Orthomode Transducer," 2002, *13th Symposium on Space THz Technology*, Cambridge MA.
- [7] Nesti, R., Private Communication, 2002, Osservatorio Astrofisico di Arcetri, Firenze, Italy.
- [8] Uher, J., Bornemann, J., Rosenberg, U., *Waveguide Components for Antenna Feed Systems: Theory and CAD*, 1993, Artech House, Norwood, MA, section 3.8, pp. 371—445.
- [9] Hewlett Packard EEsof Division, *Hewlett Packard High Frequency Structure Simulator (HFSS)*, Santa Rosa, CA 95403.
- [10] Montgomery, C.G., Dicke, R.H., Purcell, E.M., *Principles of Microwave Circuits*, 1987, IEE Electromagnetic Waves Series, vol. 25, Peter Peregrinus, London, chapter 12. (First published 1948, MIT Radiation Laboratory Series, Vol. 8, McGraw-Hill, New York.)

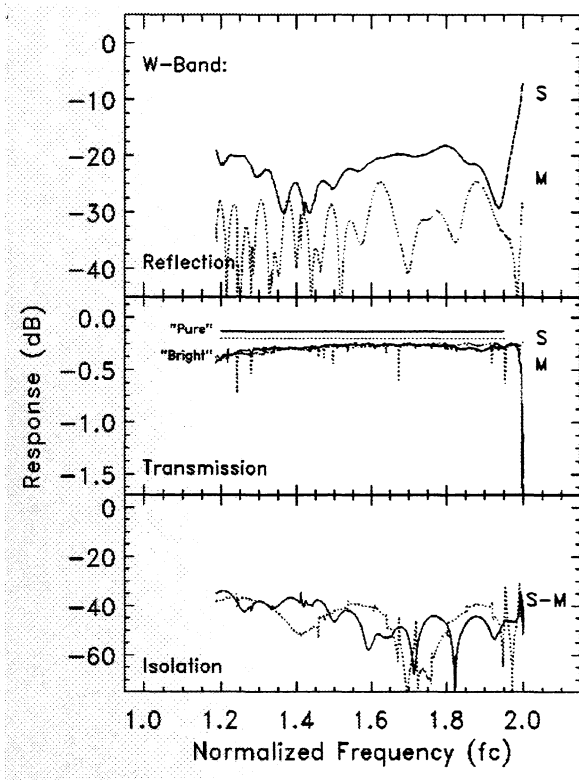


**Figure 2: WR10.0 OMT ( $f_c=59.01$  GHz).** The solid and dashed lines are respectively the side- and main-arm responses for reflection and transmission. The solid isolation line is with a load on the common-arm; the dashed line is with a short on the common-port.

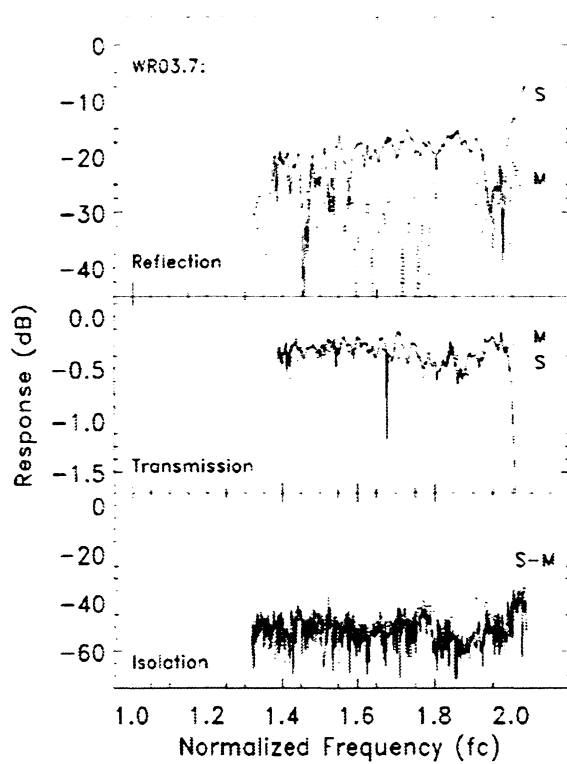


**Figure 3: WR03.7 OMT ( $f_c=159.6$  GHz).** The solid and dashed lines are respectively the side- and main-arm responses for reflection and transmission. The solid isolation line is with a load on the common-arm; the dashed line is with a short on the common-port.

Wave Band	Output Guides [WR]	Guide Broadwall $a_0$	Sidearm: Power Combiner Angle	Power Combiner Transformer Ratio	Flange Geometry	OMT Mass [gm]	Spit-Block Envelope L x W x H [mm <sup>3</sup> ]
Q ( $\lambda_0 \approx 7$ mm)	22.4	5.69 mm (0.224")	$\pi/4 : \pi/4$	0.5 : 1.0	19.1 mm (0.750") Sq	45 (Al)	44 x 28 x 26
Q ( $\lambda_0 \approx 7$ mm)	22.4	5.69 mm (0.224")	$\pi/2 : \pi/4$	0.5 : 1.0	19.1 mm (0.750") Rd.	149 (Brass)	45 x 29 x 28
W ( $\lambda_0 \approx 3$ mm)	10.0	2.54 mm (0.100")	$\pi/2 : \pi/4$	1.0 : 2.0	19.1 mm (0.750") Rd.	110 (Brass)	32 x 22 x 28
- ( $\lambda_0 \approx 1$ mm)	3.7	.94 mm (0.037")	$\pi/2 : \pi/4$	1.0 : 2.0	9.5 mm (0.375") Rd.	24 (Brass)	14 x 17 x 14

**Table 1: Orthomode Junction Design and Layout Summary.**

## APPENDIX A: Waveguide Loss Considerations

Since standard flanges do not scale with guide size, in practice, the flange interface area can significantly influence the overall component size. For wavelengths greater  $\sim 5$ mm, physically small compensation structures are desirable to minimize overall device mass and volume. For wavelengths less than  $\sim 5$ mm, physically large matching and potentially overmoded structures are desired to control loss and improve overall manufacturability. With adequate attention to detail, the benefits of reduced ohmic loss can be realized while mitigating the potential spurious effects of mode conversion [5].

In light of these considerations, we briefly consider the scaling laws for the ohmic component of the loss which result from a finite electrical conductivity,  $\sigma$ . In limit the skin depth,  $\delta = (2/\omega\mu\sigma)^{1/2}$ , is small compared to the metallization thickness and wavelength, the loss can be estimated by perturbation of boundary conditions [10]. The power loss per unit length in the guide is,

$$\begin{aligned}\alpha &= -\frac{1}{P} \frac{dP}{dz} = \frac{1}{P} \operatorname{Re} \left\{ \int_{\text{cross section}} \vec{S} \cdot \hat{n} \, dA \right\} \\ &\cong \frac{R_s}{2P} \oint_{\text{walls}} dl \left| \vec{H} \times \hat{n} \right|^2\end{aligned}$$

For the dominate mode for a rectangular guide with broadwall dimension  $a_o$  and sidewall height  $b_o$ ,

$$\begin{aligned}\alpha &= \frac{R_s}{2P} \left[ \int_{\text{broadwall}} dx \left( \frac{\beta^2}{k_c^2} \sin^2 k_c x + \cos^2 k_c x \right) + \int_{\text{sidewall}} dy \right] \\ &= \frac{2R_s}{\eta} \left[ \frac{1}{2b_o} + \left( 1 - \frac{\beta^2}{k^2} \right) \frac{1}{a_o} \right] \frac{k}{\beta}\end{aligned}$$

where  $k = (\epsilon\mu)^{1/2} \omega$ , the propagation constant is  $\beta = (k^2 - k_c^2)^{1/2}$ , and  $k_c = \pi/a_o$  is the mode cutoff wavevector. For a good metal, the ratio of the surface resistivity,  $R_s = 1/\sigma\delta$ , over the impedance of free space,  $\eta = (\mu/\epsilon)^{1/2}$ , is small compared to unity. It is convenient to define the following dimensionless function,

$$\begin{aligned}\xi &\equiv \frac{\pi}{2} \frac{\eta}{R_s} \frac{\alpha}{k_c} \\ &= \left( \frac{a_o}{2b_o} + 1 \right) \frac{k}{\beta} - \frac{\beta}{k}\end{aligned}$$

This allows a practical separation of the geometric and material contributions to the attenuation for the dominate mode. This quantity is plotted in Figure 4 with the guide aspect ratio as a parameter. As the sidewall height is increased, the loss is correspondingly reduced by accepting a smaller the single mode bandwidth. This basic behavior is reminiscent of the unloaded cavity quality factor,  $Q_o$ , which in the thermal dynamic limit scales as the characteristic size of the system in wavelengths. We recall, for a cavity with TE<sub>10</sub> illumination,

$$1/2Q_o \cong \frac{R_s}{4\omega U} \left[ \int_{length} dz \oint_{walls} dl \left| \vec{H} \times \hat{n} \right|^2 + 2 \int_{ends} dA \left| \vec{H} \times \hat{n} \right|^2 \right]$$

$$= \frac{2R_s}{\eta} \left[ \frac{1}{2k b_o} + \left( 1 - \frac{\beta^2}{k^2} \right) \frac{1}{k a_o} + \left( \frac{\beta^2}{k^2} \right) \frac{1}{k l_o} \right]$$

where  $l_o$ , the length of the rectangular waveguide, imposes a discrete symmetry on the resonant responses. In the limit the cavity length tends to infinity, the contribution of the ends relative to the sidewalls drops. Similarly, a discrete excitation spectrum is possible in the limit  $b_o$  is large enough to allow multimode propagation. This general picture can be extremely useful in considering the effects of transmission and isolation resonances in the multi-mode limit. In practice, the necessity to control these effects presents a challenge for achieving ultra low-loss wide-band performance for guide aspect ratios significantly larger than 1:1 without the use of mode filters in homogenous structures.

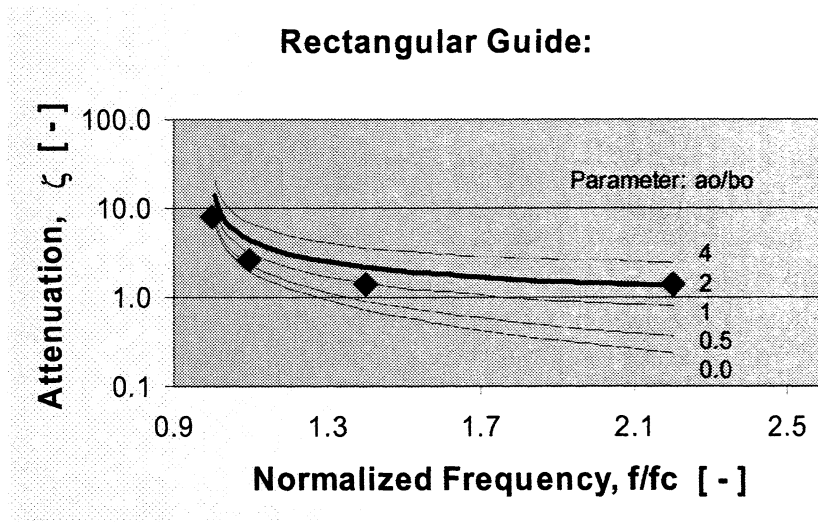


**Figure 4: Normalized Waveguide Attenuation versus Frequency.** The geometric dependence of attenuation constant is plotted with the broadwall over guide height as a parameter. The bold line depicts the normalized attenuation of a standard 2:1 guide. The diamonds indicate the onset of TE<sub>11</sub> and TM<sub>11</sub> mode propagation for the aspect ratios indicated.